

## P4.3

### AN UPATE ON THE FAA AVIATION WEATHER RESEARCH PROGRAM'S *IN SITU* TURBULENCE MEASUREMENT AND REPORTING SYSTEM

Larry B. Cornman\*, Greg Meymaris and Martha Limber  
Research Applications Program  
National Center for Atmospheric Research  
Boulder, CO.

## 1. INTRODUCTION

Under the sponsorship of the Federal Aviation Administration, work was begun in the early 1990's at the National Center for Atmospheric Research to develop and deploy an *in situ* turbulence measurement and reporting system for commercial aircraft. The concept was to use existing sensors, avionics and communication networks to produce and disseminate a state-of-the-atmosphere turbulence metric – the eddy dissipation rate (EDR). These data would then be used by a variety of users for operational and scientific purposes. Operational users include pilots, airline dispatch and meteorology personnel, aviation forecasters, and air-traffic personnel. Furthermore, these data would also be used by the turbulence research and development community for building and improving turbulence detection, nowcast and forecast products.

The EDR reports are intended to augment the existing turbulence pilot reporting data. As is well-known, these pilot reports are subjective measures of the aircraft's response to the turbulence, as opposed to quantitative, state-of-the-atmosphere measurements. Furthermore, pilot reports are sporadic in space and time, and very few null reports are made. The EDR reporting system was designed to address many of the deficiencies with pilot reports. That is, to provide routine and quantitative measurements of atmospheric turbulence intensity levels – including null reports. It should be noted that to save communications costs, some aircraft may be configured to generate EDR reports on an "event-driven," as opposed to routine basis.

Two principal algorithms have been developed to measure the eddy dissipation rate (EDR) from on-board data. The first method uses vertical accelerations and a mathematical model of the aircraft response to turbulence in order to estimate EDR values, whereas the second method uses a calculation of the vertical wind component. A brief description of these methods is presented, along with a discussion of quality control methods that have been developed. The status of the deployment of the EDR reporting system is presented, followed by a review of the ongoing verification activities. Finally, a brief introduction is given regarding the use of EDR reports in the development and verification of a radar-based turbulence detection product, as well as model-based nowcast and forecast products.

## 2. EDR ESTIMATION METHODS

Two methods have been developed to estimate EDR values from commercial aircraft, a vertical accelerometer-based method and a vertical wind-based method.

### 2.1 Accelerometer-based method

The accelerometer-based method is described in Cornman, et al. (1995). It utilizes basic linear system input-output relationships. That is, given the power spectral density of an input field and the frequency response function of the process, the power spectral density of the output process is prescribed. In this case, the input spectrum is that of the vertical velocity field and the output spectrum is that for the aircraft's vertical acceleration. The modulus

---

\*Corresponding author address: Larry B. Cornman, National Center for Atmospheric Research, P.O. Box 3000, Boulder, CO 80307-3000; email: cornman@ucar.edu

square of the frequency response function provides the relationship between the two:

$$\phi_z(f) = |H_{zw}(f)|^2 \phi_w(f) \quad (1)$$

Integrating both sides between zero and infinity gives the variance of the output process,

$$\sigma_z^2 = \int_0^{\infty} \phi_z(f) df = \int_0^{\infty} |H_{zw}(f)|^2 \phi_w(f) df$$

If a von Karman or Kolmogorov model (Cornman, 1995) for the input spectrum is chosen, then the spectrum is product-separable in the eddy dissipation rate (to the 2/3<sup>rd</sup>s power),

$$\phi_w(k_x) = \varepsilon^{2/3} \psi_w(k_x) \quad (2)$$

where,  $k_x$  is the wavenumber in the direction of motion (assumed to be the x-axis). Since the theoretical spectra are defined in terms of wavenumbers, a conversion to temporal frequency is required. Assuming that spatial variables in the direction of the mean flow can be replaced with temporal ones (i.e., Taylor's hypothesis is valid),  $k_x = 2\pi f / \bar{V}_x$ ,

$$\phi_w(f) = \varepsilon^{2/3} \frac{2\pi}{\bar{V}_x} \psi_w(k_x = 2\pi f / \bar{V}_x)$$

where  $\bar{V}_x$  is the mean value of the component of the aircraft's velocity (with respect to the local air mass) along the flight track. Usually, this is approximated by a temporal average of the true airspeed.

Therefore, the variance of the vertical acceleration spectrum is given by

$$\sigma_z^2 = \varepsilon^{2/3} \int_0^{\infty} |H_{zw}(f)|^2 \frac{2\pi}{\bar{V}_x} \psi_w(k_x = 2\pi f / \bar{V}_x) df \quad (3)$$

and hence, the eddy dissipation rate to the 2/3<sup>rd</sup>s power is given by

$$\varepsilon^{2/3} = \sigma_z^2 / I \quad (4)$$

where  $I$  is the integral in the previous equation. In practice, the variance of the vertical acceleration is computed in the time-domain, after the application of a band-pass filter. The filter is intended to remove low-frequency aircraft maneuver-induced accelerations and high-frequency flexible-mode accelerations. Furthermore, the frequency range of the filter is chosen to ensure (as best as possible) the applicability wind spectrum model. Note that since the frequency-domain wind spectrum is functionally dependent on the airspeed, the cut-offs for the band-pass filter should also be functions of the airspeed. The frequency-domain response function for the band-pass filter is then used in Eq. (3).

Another approach is to use Eqs. (1) and (2) to give

$$\phi_z(f) = \varepsilon^{2/3} |H_{zw}(f)|^2 \psi_w(f)$$

Then a single parameter maximum-likelihood method (Smalikhov, 1997) can be used to estimate the eddy dissipation rate to the 2/3<sup>rd</sup>s power:

$$\varepsilon^{2/3} = \frac{1}{N} \sum_{i=1}^N \frac{S_z(f_i)}{|H_{zw}(f_i)|^2 \psi_w(f_i)} \quad (5)$$

where  $S_z(f)$  is the measured power spectrum of the vertical acceleration time series. The summation is taken over a range of frequencies commensurate with those used in the band-pass filter mentioned above. Furthermore, as above, these frequencies will depend on the airspeed.

In either method, a significant problem resides in an accurate representation of the aircraft's vertical acceleration response function. In Cornman (1995), a mathematical model for the aircraft – including a simple autopilot model – is presented. Nevertheless, this requires certain knowledge about the specific aircraft. Furthermore, the aircraft response function

is dependent on the given flight conditions, e.g., altitude, mass and airspeed. In some cases, the aircraft response function may be available from the manufacturer or via aircraft simulators. Obviously, if these data are available, they are preferable to the mathematical modeling approach.

## 2.2 Wind-based method

The wind-based EDR estimation algorithm is a more direct approach than the accelerometer-based technique. In this method, estimates of the vertical wind are made and then a frequency-domain, single-parameter maximum-likelihood calculation is used to estimate the eddy dissipation rate to the  $2/3^{\text{rds}}$  power,  $\varepsilon^{2/3}$ . This method obviates the need for obtaining or calculating the aircraft frequency response function.

The vertical wind estimate is given by (Wingrove and Bach 1994):

$$w = \dot{z} + V_T [\cos(\psi) \sin(\alpha_B) \cos(\theta) - \cos(\alpha_B) \sin(\theta)] \quad (6)$$

where,  $\dot{z}$  is the vertical component of the inertial velocity vector (positive along the gravitational vector),  $V_T$  is the true airspeed,  $\psi$  is the roll angle,  $\theta$  is the pitch angle, and  $\alpha_B$  is the body-axis angle-of-attack. Note that it is assumed that the sideslip angle is zero in this equation. This parameter is typically only available on research aircraft, and since it is usually small, it is set to zero in Eq. (6). The power spectrum of the vertical wind estimates are then used with a maximum-likelihood method similar to Eq. (5),

$$\varepsilon^{2/3} = \frac{1}{N} \sum_{i=1}^N \frac{S_w(f_i)}{\psi_w(f_i)} \quad (7)$$

where  $S_w(f)$  is the measured power spectrum of the vertical wind estimates. The summation is performed over the range of frequencies such that the wind spectral model is assumed to hold. As with the

accelerometer-based method, this range of frequencies will depend on the true airspeed.

In some cases, not all the parameters in Eq. (6) are available on the aircraft at the same update rate. Hence, an oversampling interpolation, antialiasing filtering and decimation procedure must be employed to resample all the fields at the same rate. At that point, the vertical wind time series power spectrum of the wind time series is computed. In order to accommodate the effect of the antialiasing filtering, Eq. (7) can be modified to yield,

$$\varepsilon^{2/3} = \frac{1}{N} \sum_{i=1}^N \frac{S_w(f_i)}{|H_a(f_i)|^2 \psi_w(f_i)}$$

where  $|H_a(f_i)|^2$  is the modulus square of the transfer function for the composite antialiasing filter effect on the vertical wind calculation.

## 3. EDR REPORTING

In either EDR estimation method, the temporal windows over which the  $\varepsilon^{2/3}$  calculations and reports are made must be specified. The choice of the window sizes is a compromise between resolving discrete turbulence events and transmission costs. For aircraft in cruise, a nominal one-minute reporting interval has been used. (The reporting interval for ascent and descent phases of flight is typically different than for the cruise mode.) Within this reporting window, sub-windows are chosen for the calculation of the  $\varepsilon^{2/3}$  estimates. For the time-domain version of the accelerometer-based method, described subsequent to Eq. (4) above, each  $\varepsilon^{2/3}$  estimate is calculated over a 10-second sliding window. This window is updated at every new sample of the accelerometer data (e.g., 4 or 8 Hz.). This procedure provides for a very fine resolution of the  $\varepsilon^{2/3}$  values; however, the estimates are highly correlated. This procedure was designed to simplify the real-time on-board processing. For the frequency-domain maximum likelihood methods, a nominal 10-second window is used for the EDR estimates, with a nominal

$\frac{1}{2}$  overlap sliding window. This approach produces a time series of  $\varepsilon^{2/3}$  values that are not overly correlated, but at the expense of high temporal resolution.

The choice of window-length and EDR update is a compromise between having enough resolution to capture discrete events and having enough samples in the window to provide stable computational statistics. The analysis of large-amplitude, discrete turbulence encounters indicates that the temporal duration at typical commercial transport cruise speed is on the order of 5-15 seconds. Thus, the 10-second window with  $\frac{1}{2}$  overlap used with the wind-based method seems to be a reasonable compromise. The same can be said for the time-domain version of the accelerometer-based method; however the high sample update rate for the EDR estimates is probably not needed.

With either EDR estimation method, a time series of the  $\varepsilon^{2/3}$  values are then produced over the nominal one-minute cruise-mode reporting interval. In order to accommodate a compromise between event resolution and transmission costs, two values are ultimately sent in the EDR report: the square root of the median and square root of the 95% values of the individual  $\varepsilon^{2/3}$  estimates, over the one-minute period. In this fashion, a qualitative knowledge of whether the turbulence is relatively continuous or discrete over the one-minute time period can be ascertained. That is, if the turbulence is relatively continuous, the median and 95% values should be close in magnitude, whereas for a discrete event, the 95% value will typically be much larger than the median value. The reason for using a median and 95% value – rather than an average and peak – is to mitigate potential erroneous reports due to data quality issues. Other mitigation methods are discussed in Section 4.

### **3.1 Use of the EDR Reports to Produce Aircraft-Dependent Information**

As mentioned above, the eddy dissipation rate is a state-of-the-atmosphere turbulence intensity metric, i.e., it is an aircraft-independent measure. Nevertheless, there

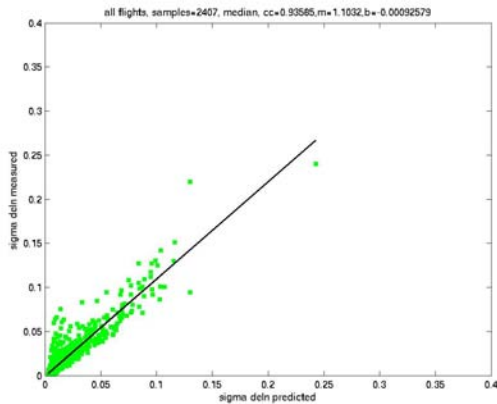
may be users, for example, a pilot, who desires an aircraft-dependent turbulence value. In order to investigate the utility of generating an aircraft-dependent measure of turbulence, an analysis was performed using high-rate data from the NASA B-757 aircraft. Eq. (4) represents the connection between an aircraft-independent measure ( $\varepsilon^{2/3}$ ) and an aircraft-dependent one ( $\sigma_z^2$ ). To simulate one-minute EDR reports from a commercial aircraft in cruise, the vertical wind data from the B-757 were used to produce median and 95%  $\varepsilon^{1/3}$  values, as described above. In a similar fashion, the median and 95% root-mean-square (rms) of the vertical accelerations was also calculated. That is, sliding 10-second windows, with  $\frac{1}{2}$  overlap, were used to calculate a time series of rms vertical acceleration values. The median and 95% value of these individual quantities were then calculated over the one-minute windows. As the aircraft was undergoing maneuvers during a number of flight segments, a high-pass filter was applied to the acceleration time series prior to computing the rms value. The median and 95%  $\varepsilon^{1/3}$  values were then scaled via  $\hat{\sigma}_z = \varepsilon^{1/3} I^{1/2}$  to produce “EDR-predicted” rms vertical acceleration estimates ( $\hat{\sigma}_z$ ).

Figure 1 is a scatterplot of the one-minute median values for the actual versus EDR-predicted rms vertical accelerations; whereas Figure 2 shows the 95<sup>th</sup> percentile values. 2407 one-minute values are shown, or approximately 40 hours of flight data. This selection of data constituted all of the time that the aircraft was above 10 kft.; which means that a wide variety of flight conditions was sampled. In both figures, a small number of points can be seen clustered above the one-to-one line, but at small EDR-predicted vertical acceleration values (lower-left corners). These points are due to the incomplete removal of all the maneuver-induced accelerations via the high-pass filter. Nevertheless, these points do not significantly affect the results, and in fact show that the EDR estimates (via the wind-based method) are insensitive to maneuvers. The correlation coefficient for the median values is 0.94 and the slope is 1.1. For the 95<sup>th</sup> percentile values, the

correlation coefficient is 0.95 and the slope is 1.2. The slight positive biases in the slopes are due to the maneuver contamination, mentioned above.

These results clearly indicate that EDR estimates can be used to calculate rms vertical accelerations for commercial transport aircraft with a high degree of fidelity. That is, the EDR reports can be used as a universal, aircraft-independent metric for communicating turbulence information between users. If a user desires an aircraft-dependent measure, it can be estimated via the relation,  $\hat{\sigma}_z = \epsilon^{1/3} I^{1/2}$ .

Recall that the integral,  $I$  is a function of the aircraft type and flight condition (mass, altitude and airspeed); hence, this information must be available at the location of the user who desires an aircraft-dependent measure. On the other hand, if an aircraft-dependent measure, such as  $\sigma_z$ , was used as the universal turbulence metric, then the parameter  $I$  would also need to be transmitted, increasing communication costs. Furthermore, an aircraft-independent measure, (such as the eddy dissipation rate), would still be required as an intermediary between two users who want aircraft-dependent information – such as in aircraft-to-ground-to-aircraft, or aircraft-to-aircraft communication.



**Figure 1.** Median values of  $\epsilon^{1/3}$  over one-minute intervals, compared with the median of the rms vertical accelerations over the same interval.

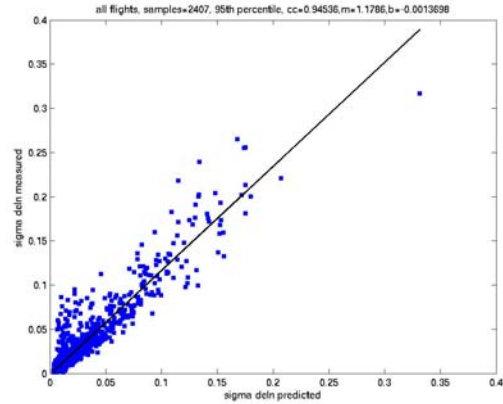


**Figure 2.** 95% values of  $\epsilon^{1/3}$  over one-minute intervals, compared with the 95% value of the rms vertical accelerations over the same interval.

#### 4. QUALITY CONTROL METHODS

Two methods are available for performing quality control (QC) on the EDR data: on-board processing and ground-processing. In either case, the desired result is an overall quality rating for the report-level EDR values.

##### 4.1 On-board QC Processing

For the accelerometer-based method, the algorithm inputs include the vertical accelerometer, true airspeed, altitude and mass data. Perfunctory tests include bounds checking, and identifying sample-to-sample jumps. More sophisticated methods, such as the Least Squares Adaptive Polynomial (LSAP, also known as Discounted Least Squares; Abraham and Ledolter 1983) can also be applied to the various time series to detect anomalies. The LSAP algorithm is a very efficient, weighted least-squares polynomial fitting method. Typically, a second-order polynomial is used, and a single parameter determines the “memory” for the weights. The weights are exponentially decreasing backwards in time, and hence the memory parameter determines the drop-off rate. LSAP provides a prediction – based on the polynomial fit – for the current time value of the data, as well as a running estimate for the standard deviation of the fit. A z-statistic is then calculated by taking the ratio of the absolute value of the difference between the current

data point and the polynomial prediction for the current time, divided by the current estimate for the standard deviation. A QC value for the current data point is then computed by mapping the z-statistic to the interval (0,1) via, for example, an exponential or Gaussian function. If there are quality problems detected with one of the input fields, a QC flag is set and transmitted as the EDR report.

For the wind-based method, there are two levels of on-board QC processing that occur: preliminary tests on the inputs to the vertical wind calculation, and more sophisticated tests on the vertical winds themselves. The preliminary tests are similar to those used above for the accelerometer-based method. The more sophisticated method has two parts. The first part uses the LSAP algorithm to provide a “first guess” QC value. With large-amplitude discrete turbulence events, the data can change from quiescent to rapidly varying in a short time period. Unfortunately, this type of abrupt change is not conducive to the continuous polynomial modeling of LSAP, and hence the use of this method may result in labeling valid turbulence data as suspect. On the other hand, data contaminants could also show a similar temporal structure. Therefore, a second stage of processing beyond LSAP is used to differentiate between the two types of processes.

The analysis of abrupt changes in data level is well-suited to wavelet analysis (Chui, 1992), especially using the Harr wavelet basis. The Harr basis is essentially a symmetrical step function centered at the current point, with a prescribed number of non-zero values before and after the point. Unfortunately, the detection of an abrupt change in the data still does not give enough information as to whether it is “real” or due to outliers. In the time-domain, the vertical acceleration time series is related to that of the vertical wind (for linear aircraft response), via the convolution integral,

$$\ddot{z}(t) = \int_{-\infty}^t h_{zw}(t-\tau)w(\tau)d\tau$$

where  $h_{zw}(t)$  is the impulse response function. It can be seen that the time series

of the vertical acceleration and the vertical wind are related in a prescribed manner. Therefore, the resolution to the ambiguity problem resides in a comparison between the vertical acceleration and vertical wind time series. Specifically, the vertical accelerations are scaled by a function which depends on the aircraft response, (which in turn is a function of flight condition). It is assumed that for a real turbulence event, the scaled vertical accelerations and the vertical winds should be closely coupled in both time and magnitude; whereas for a significant outlier in the wind time series, their values should be considerably different.

The scaled vertical acceleration time series and the vertical wind time series are then processed with Harr wavelets. An algorithm which compares the outputs of the Harr wavelets along with the LSAP output is then used to determine a final QC value for the given vertical wind sample. If a single outlier in the vertical wind is detected, an interpolation between neighboring points can be performed. Nevertheless, as this interpolation can affect the  $\varepsilon^{2/3}$  estimate, the overall confidence in the  $\varepsilon^{2/3}$  value is lowered. If a number of sequential data points are deemed to be outliers, then the  $\varepsilon^{2/3}$  estimate for that window is flagged as being bad.

Two examples of the LSAP/wavelet QC processing are shown in the following figures. In the first example, a single-point spike in the vertical wind time series is presented. In the second case, a significant, but real step in the vertical wind is shown. Figure 3 is a time series of the vertical wind (blue) and the vertical accelerometer (red). Clearly, the single-point spike in the wind is an outlier. Figure 4 shows the ratio between wavelet information calculated from the scaled vertical acceleration and the vertical wind. In this example, this ratio is very small, indicating the vertical acceleration time series does not “corroborate” the spike in the vertical wind. Figure 5 illustrates the stand-alone LSAP QC value (red) and the wavelet-modified LSAP QC value (blue). In this case, LSAP does an excellent job of identifying the outlier, and hence the two QC values are essentially the same.

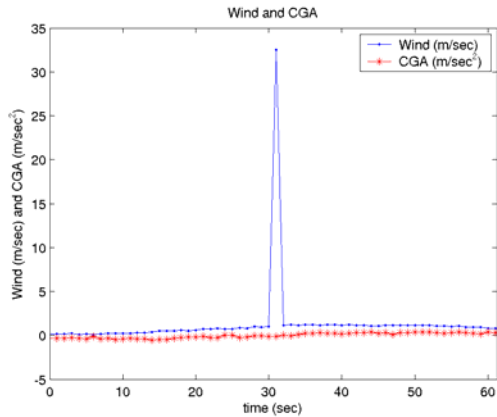


**Figure 3.** Time series of vertical accelerations (red) and vertical wind (blue) for example case 1.

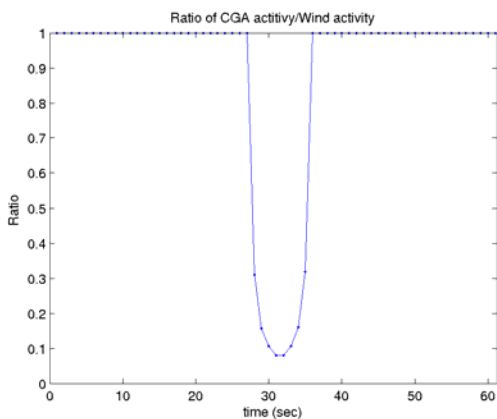


**Figure 4.** Time series of the ratio of wavelet-derived quantities from the vertical acceleration to those from the vertical wind.

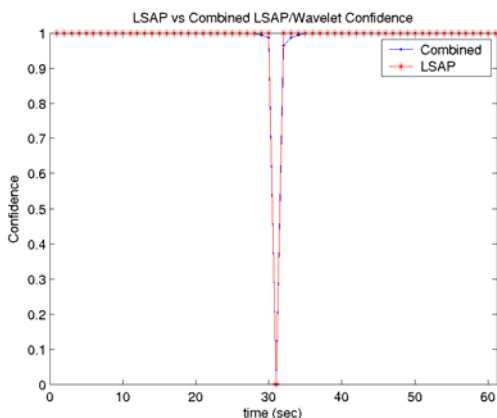


**Figure 5.** QC values from the stand-alone LSAP processing (red) and the wavelet-modified LSAP processing (blue).

In the second example case, shown in Figure 6, a number of large jumps in the vertical wind can be seen. This data sequence was from a relatively significant turbulent encounter; hence the final result of the QC algorithm should not label them as outliers. Consider the  $10 \text{ ms}^{-1}$  jump in the vertical wind at around 15 seconds in Figure 6. At the same time, there is a corresponding large jump in the vertical acceleration. In Figure 8, it can be seen that the stand-alone LSAP QC value is quite small at this time. This is because LSAP assumes that the polynomial model (here, quadratic) computed from the data preceding the jump will continue into the future. LSAP also considers the next two points to be outliers. After three consecutive outliers, the LSAP model is re-initialized and hence the stand-alone LSAP QC values return to “normal” levels. Figure 7 illustrates the “wavelet-ratio” function described above. At 15 seconds in the time series, the ratio values are close to one, indicating that the vertical acceleration time series is corroborating the jump in the vertical wind. This information is then used to modify the LSAP QC values, as can be seen from the blue curve in Figure 8. Notice the large values of the wavelet ratio function between 20 and 25 seconds in Figure 7. This is due to maneuver-induced accelerations that do not correspond to appreciable changes in the vertical wind, which implies that if there is an outlier in the winds during a maneuver, this QC processing method may fail. Nevertheless, if the outlier is a large spike, as in the previous example, it would most likely be caught.

Finally, it should be pointed out that if a sensor “locks on” to a bad (but not physically unreasonable) value, the QC methods previously discussed may not identify it as being in error. Hence, further analysis of the EDR reports may be required to address this type of problem. An example of additional QC processing is discussed in the next section.

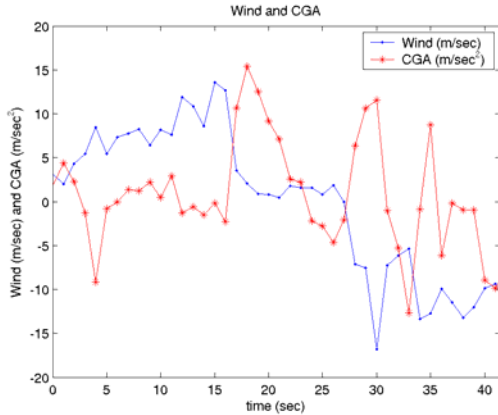


**Figure 6.** Time series of vertical accelerations (red) and vertical wind (blue) for example case 2.

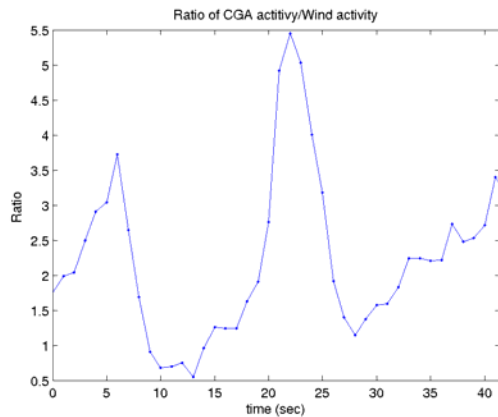


**Figure 7.** Time series of the ratio of wavelet-derived quantities from the vertical acceleration to those from the vertical wind.

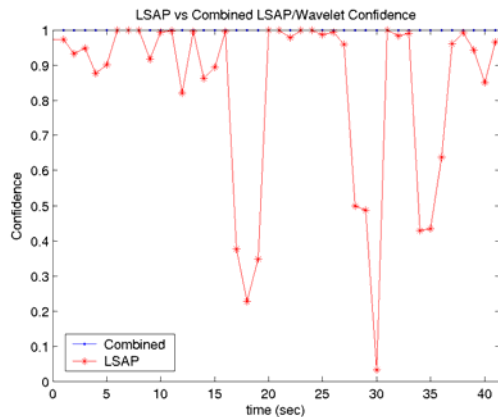


**Figure 8.** QC values from the stand-alone LSAP processing (red) and the wavelet-modified LSAP processing (blue).

## 4.2 Ground-based QC Processing

In addition to the on-board quality control processing, a variety of checks are performed on the EDR reports after they are received on the ground. (Note that similar QC checks would need to be performed if the data are being cross-linked between aircraft.) Figure 9 and Figure 10 illustrate an important aspect of this QC procedure. Figure 9 shows the time series of EDR reports from a flight on 10 November 2003. The small points are the 95% values, whereas the colored circles are the median values. The colors are indicative of the altitude. The large EDR values towards the middle of the plot could be interpreted as an encounter with a significant turbulence event. However, this particular tail number was intermittently reporting EDR values that were clearly in error. This can be seen in Figure 10, which shows the EDR values from the same aircraft, for a flight five days prior to the one on 10 November. Clearly, having knowledge about the previous behavior of EDR reports from a specific aircraft is very valuable in assessing the quality of reports as they are received. This is easily accomplished on the ground, where a database of all reports can be established, but would be more problematic when considering turbulence reports being cross-linked between aircraft. That is, each aircraft would need to have a database regarding the previous quality of data on the aircraft from which it may currently be receiving turbulence reports.

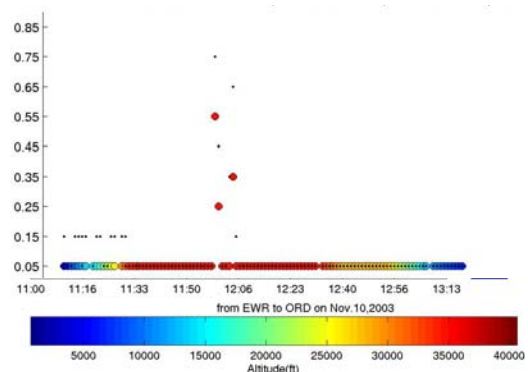


**Figure 9.** Time series of EDR reports from a flight on 10 November 2003. It is hard to tell whether the large values are real or outliers.

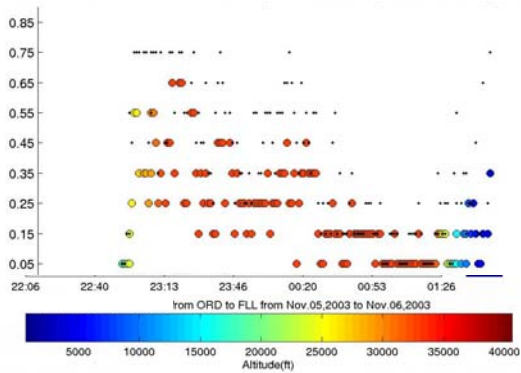


**Figure 10.** Time series of EDR values from the same aircraft whose data is shown in Figure 9. This flight is 5 days prior to the 10 November flight.

There are two aspects to the ground-processing of the EDR reports: near real-time, and post-processing. In the first application, the data are to be used for operational decision-making, which includes the use of the EDR reports by airline dispatch and meteorology staff, and aviation forecasters. The data will also be used in automated turbulence detection, nowcast and forecast applications. In the post-processing application, the data is primarily used for the development and verification of turbulence detection, nowcast and forecast products. Obviously, with near real-time processing, only data up to the current time can be used to ascertain the quality of the EDR reports. This limits the ability to determine whether a given aircraft has a faulty sensor, and implies that there is a potential for false alerts in these circumstances – unless other data is available for cross-validation. For example, if the first indication of a sensor problem was from the flight whose data is shown in Figure 9, it would be very difficult, if not impossible, to determine whether the large EDR values are real. In such a case, other data might be used to try and ascertain whether the reports are valid. These other sources of data could include the WSR-88D radar turbulence detection product (Williams, et al. 2004), the analysis product from the Graphical Turbulence Guidance product (Sharman, et al., 2004), EDR reports from other nearby aircraft, or pilot reports. Examples of inter-comparisons between

EDR reports and these other sources of turbulence information are presented in the next section.

## 5. PROGRAM STATUS

Starting in 1997, the implementation of the first-generation accelerometer-based EDR algorithm was begun on United Airlines aircraft. A total of 199 aircraft, B737s and 757s, currently have the algorithm installed; however, due to cost savings, only the 737s are currently providing routine EDR reports. Starting in 2005, the wind-based algorithm will be installed on 160 aircraft from Delta airlines and 93 aircraft from Southwest Airlines. In the following sections, a sampling of the current activities associated with the United Airlines deployment is discussed, including verification efforts and the use of the EDR reports in the development and verification of radar- and model-based turbulence products.

### 5.1 Verification Activities

The algorithm that has been implemented on the United Airlines aircraft is based on accelerometer data. Improvements to this first-generation accelerometer-based version exist, (including better aircraft response data, band-pass filtering and quality control processing), but have not been deployed. In fact, it is assumed that all future implementations will be based on the vertical wind, maximum-likelihood algorithm. Nevertheless, these accelerometer-based EDR data give a good idea as to the benefits of the turbulence reporting concept.

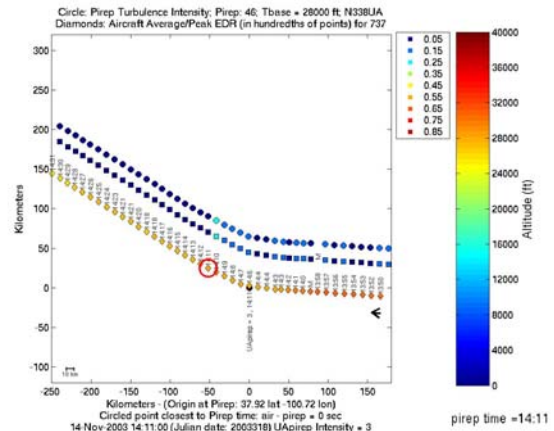
The EDR reports from the United Airlines deployment are undergoing verification by a comparison to pilot reports of turbulence as well as occasional passenger reports. Figure 11, Figure 12, and Figure 13 show a spatial series of EDR reports for portions of three different flights. These cases were chosen because there was a pilot report of turbulence from the specific flight. There are two locations indicated for the pilot reports: the red circle shows the location along the flight track at the time given in the pilot report; whereas, the black dot indicates the aircraft location given in the pilot report. Note that these two locations do not always match. The actual flight track is indicated by

the color-coded (by altitude) diamonds and the two parallel tracks are the median and 95%  $\varepsilon^{1/3}$  values, (color code in the upper right). The arrow gives the direction of the flight track.

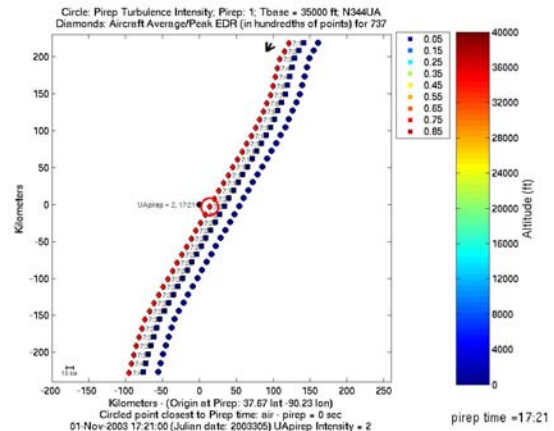
In Figure 11, a reasonably good match is seen between the pilot report (“light-to-moderate”) and the  $\varepsilon^{1/3}$  report (0.25). There is a discrepancy between the locations of the encounter as given by the time in the pilot report versus the location given in the pilot report. In analyzing these data, it has been seen that this type of divergence occurs relatively often. Figure 12 illustrates a case where there is a difference between the pilot report (“light”) and the  $\varepsilon^{1/3}$  report (0.05). Without further information, this discrepancy cannot be resolved. However, it should be noted that since the  $\varepsilon^{1/3}$  values are binned in increments of 0.1, an  $\varepsilon^{1/3}$  value that lies between zero and 0.1 would be reported as 0.05, and this could be a source of the difference. In future implementations, it is envisioned that a finer resolution, at least at the lower EDR values, might be employed. Finally, Figure 13 illustrates a more extreme example of the problem mentioned above regarding the positional inaccuracies in the pilot reports. The pilot report shown in this figure is from the same flight as the EDR reports. Nevertheless, the location of the aircraft given in the pilot report is over 100 km from the actual flight path. Besides all of the subjectivity inherent in the turbulence pilot reports, this type of inaccuracy is yet another motivation behind the deployment of the EDR reporting system.

Figure 14 and Figure 15 present a comparison between EDR reports and turbulence “passenger reports” for two different flights. The passenger recorded a running evaluation of the turbulence intensity for the flights. The turbulence levels used by the passenger were: “null” (0), “null-to-light” (1), “light” (2), “light-to-moderate” (3), and “moderate” (4). Dashed lines between values indicate a constant intensity level between samples. In both examples, there is a reasonable, though not one-to-one correspondence between the passenger and EDR reports. As mentioned above, the

coarse resolution between the EDR levels may contribute to some of this discrepancy. It has been noted that with this first version of the accelerometer-based EDR algorithm, it is not uncommon to find relatively large EDR values during the climb-out and approach phases of flight. This problem can clearly be seen in Figure 14. Furthermore, the on-board quality control algorithm often flags the EDR reports at these low altitudes (see the line just above the time field in the figures).



**Figure 11.** Spatial series of EDR reports illustrating a good match between the pilot report (“light-to-moderate”) and the EDR values.



**Figure 12.** Spatial series of EDR reports illustrating a discrepancy between the pilot report (“light”) and the EDR values.

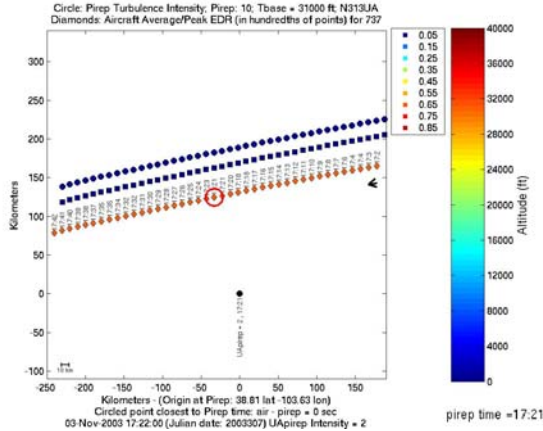


**Figure 13.** Spatial series of EDR reports illustrating one of the problems in using pilot reports for verification work. The location given in the pilot report is approximately 100 km from the actual flight track.

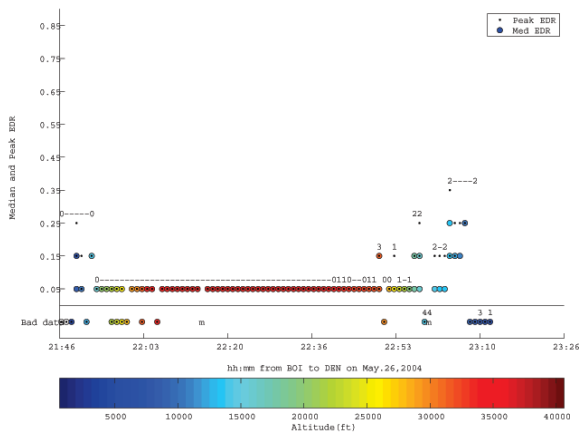


**Figure 14.** Comparison between EDR reports and “passenger reports.”

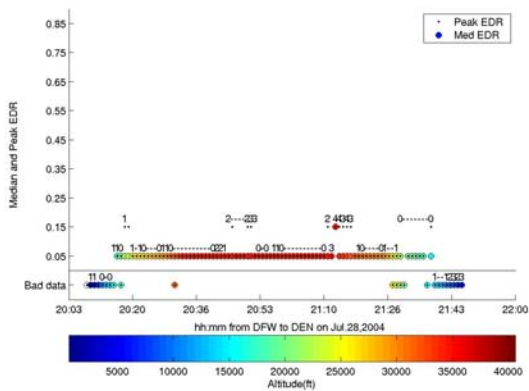


**Figure 15.** Comparison between EDR reports and “passenger reports.”

## 5.2 Use of the EDR Reports with a Ground-based Radar Turbulence Detection Algorithm

A turbulence detection product is being developed for use with ground-based Doppler radars (Williams, 2004). As part of the algorithm verification, a number of data sources are being used, one of which is the EDR reports. In the future it is assumed that the EDR data will be integrated with the radar data, as well as with numerical model data to produce a combined detection, nowcast and forecast product for in-cloud turbulence. In the following figures, a case study is presented which demonstrates the utility of the EDR reports in the development and verification of the radar turbulence product.

Figure 16 illustrates the time series of EDR reports for a flight between Chicago and Salt Lake City on November 18 2003. Notice the three instances of elevated EDR values between 00 UTC and 01 UTC. The aircraft is in level cruise at 31 kft during this time. Figure 17 is a composite reflectivity field for 31 kft using four nearby WSR-88D radars. The three turbulence encounters can be seen in this figure: in east-central and western Iowa, and in eastern Nebraska. Note that the reflectivity values are quite low, and in fact the western-most encounter is in clear air. Note that, at these reflectivity levels, airborne radar would not be indicating anything that would be of concern to the pilot. Figure 18 shows the EDR values produced by the prototype radar detection algorithm, showing good agreement for the two in-cloud encounters.

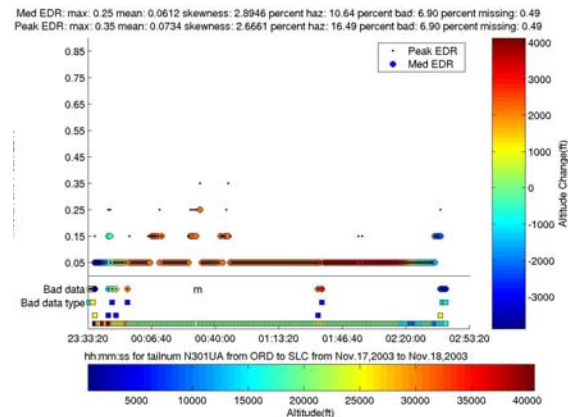


**Figure 16.** Time series of EDR reports for the 18 November 2003 flight between Chicago and Salt Lake City.

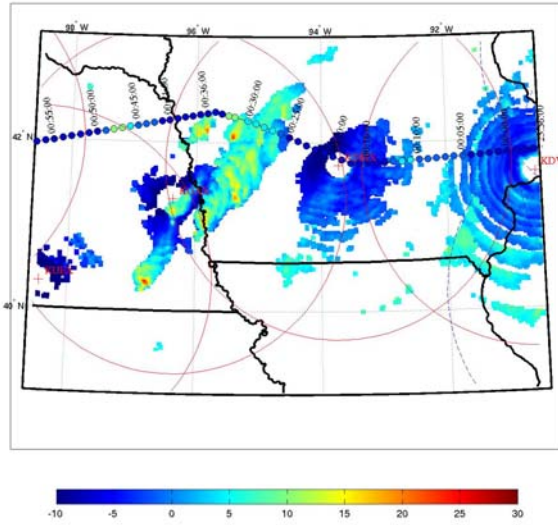


**Figure 17** Reflectivity in dBZ for the 18 November 2003 flight.

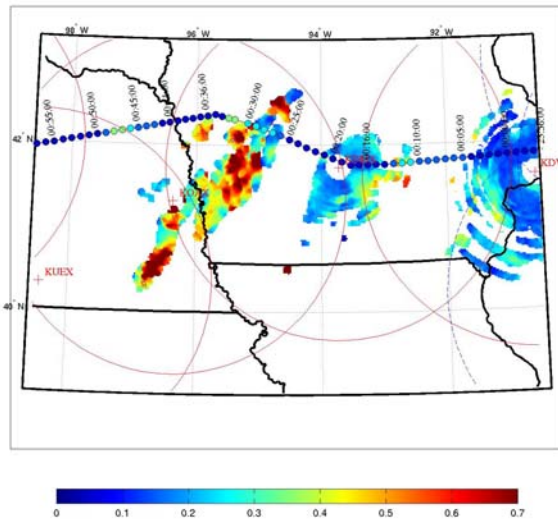


**Figure 18** Comparison of EDR values from the aircraft reports and the WSR-88D algorithm, for the 18 November 2003 flight. Valid time for the radar data is 00:30 UTC.

### 5.3 Use of the EDR Reports with the Graphical Turbulence Guidance Product

The Graphical Turbulence Guidance (GTG) product (Sharman, 2004) is an automated turbulence nowcast and forecast

diagnostic system that is used operationally by aviation forecasters. The current operational product is designed for forecasting clear-air turbulence above 20 kft; however, development efforts are underway to extend the clear-air product to lower altitudes, as well as to include turbulence due to convection. GTG uses the output of an operational numerical weather prediction model (RUC) to generate a number of turbulence diagnostics.

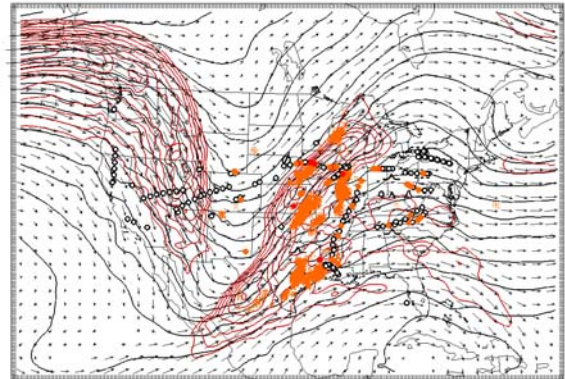
In the current operational version, these diagnostics are merged in a weighted fashion by using turbulence pilot reports at all flight levels above 20 kft to help set the weights. That is, diagnostics that correspond best to the pilot reports are given higher weights in the merging process. Furthermore, as there are a limited number of pilot reports at any given time, the weighting scheme is applied globally to the model grid. As mentioned above, there are a number of drawbacks to the use of pilot reports, and hence efforts have been initiated to use the EDR reports to augment the pilot reports within GTG. One advantage of the routine reporting of turbulence is the increased spatial and temporal coverage over event-based reporting – such as occurs with pilot reports. Routine reporting of turbulence will allow for localized weighting schemes in GTG, which should improve the overall performance. In the following, an example is presented which illustrates how the EDR reports will be useful in the next-generation GTG product.

Figure 19 shows the RUC-20 model analysis field for 31 kft (pressure altitude using a standard atmosphere), valid at 00 UTC. Overlaid is lightning data for that same time period, plus and minus one hour. Note that this is the same case as was discussed above in the context of the WSR-88D algorithm efforts. The black contour lines show the altitude of the constant pressure surface, and the red lines are contours of the horizontal velocity field. The EDR reports at 31 kft (pressure altitude; plus or minus 500 ft), and for 00 UTC (plus or minus one hour) are overlaid. Furthermore, the pilot reports at 31 kft (pressure altitude; plus or minus 500 ft), and for 00 UTC (plus or minus 1.5 hours) are also overlaid.

One of the promising new diagnostics being developed for GTG is based on a structure function analysis of the model velocity grids (Frehlich and Sharman, 2004). This diagnostic produces an EDR field, albeit one that is averaged over the spatial scales of the model grid. An example of this EDR diagnostic – for the horizontal structure function – is shown in Figure 20. Note that the enhanced levels of turbulence that are diagnosed in the regions with large gradients in the horizontal wind. Figure 21 is a blow-up of the data in Figure 20, for a geographical region that includes the one discussed in the previous section. Note the three EDR encounters from the Chicago to Salt Lake City flight, going east to west across Iowa and then into Nebraska. As discussed in the previous section, the two eastern-most encounters were in cloud, whereas the western-most one was in clear air. It can be seen that the EDR diagnostic picks up the three events, though it corresponds best with the western-most two with respect to intensity level. Figure 22 shows the merged GTG product for the same region and time period, as seen in Figure 21. (The GTG product output is a scaled intensity level between zero and one, the blue colored region is for “light” turbulence, the yellow color indicates “moderate,” and the red color indicates “severe” turbulence.) Clearly, other diagnostics in the GTG product are picking up turbulent features to the east of those predicted by the single horizontal structure function EDR diagnostic algorithm. Note that there is a null pilot report just to the west of the western-most encounter; as well as three moderate and three light pilot reports in the eastern-most portion of the figure (more easily discerned in Figure 20).

As mentioned above, the merging procedure in the current operational GTG product is based on the association between the individual diagnostics and the pilot reports. Hence, the lack of correspondence between the EDR diagnostic and the pilot reports results in the downgrading of this diagnostic’s input to the overall GTG field. Specifically, this result can be seen with the two western-most turbulence encounters on the Chicago to Salt Lake City flight. If, on the other hand, the EDR reports were used in a localized weighting algorithm within GTG, a

better overall diagnostic field would have resulted.



**Figure 19.** RUC-20 model analysis field for 31 kft, valid at 00 UTC, with lightning data overlaid.

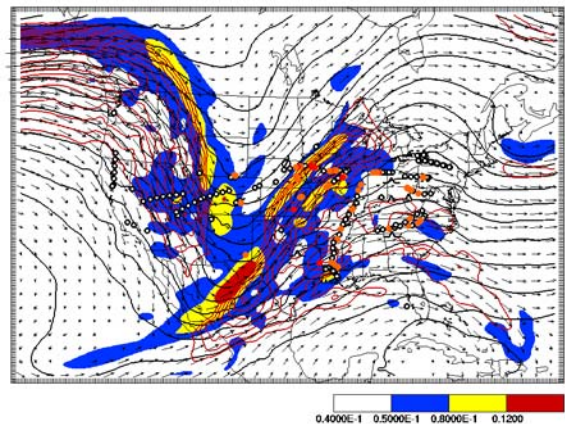


**Figure 20.** Model-based EDR diagnostic field for 31 kft, valid at 00 UTC. EDR reports are shown as open circles ( $\epsilon^{1/3} = 0-0.1$ ), orange (0.1-0.2), and red (0.2-0.3). Pilot reports for that flight level are also shown.

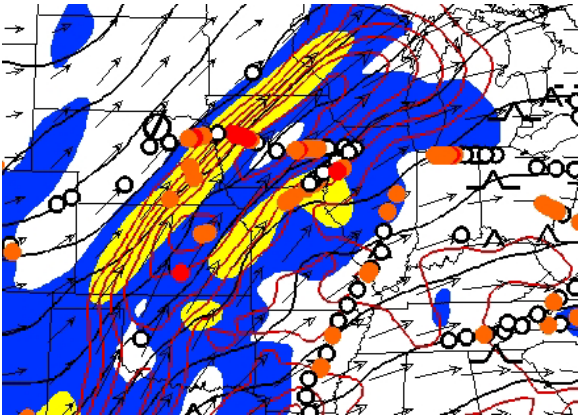


Figure 21. Blow-up of the data in Figure 20.

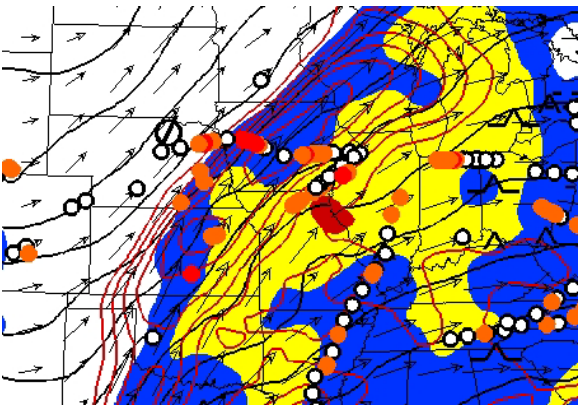


Figure 22. Same as for Figure 21, but for the merged GTG diagnostic product.

## 6. CONCLUSION

The *in situ* turbulence measurement and reporting system is an ongoing effort within the FAA's Aviation Weather Research Program. A great deal of progress has been made in the recent past, including algorithm development, the implementation of a first-generation accelerometer-based algorithm on 199 United Airlines aircraft, and the preparation for deployment of the next-generation wind-based algorithm on a number of aircraft from Delta and Southwest Airlines. Furthermore, verification activities are underway, comparing the results of the United Airlines deployment with pilot and passenger reports. Finally, investigations have been initiated into how the EDR reports can be used in concert with radar-based turbulence detection products, as well as with the GTG turbulence nowcast and forecasting product. It is hoped that the use of the EDR reports from commercial aircraft

will provide valuable assistance in reducing injuries associated with turbulence encounters.

## ACKNOWLEDGEMENT

This research is in response to requirements and funding by the Federal Aviation Administration (FAA). The views expressed are those of the authors and do not necessarily represent the official policy or position of the FAA.

## REFERENCES

Abraham, B. and J. Ledolter, 1983: *Statistical Methods for Forecasting*. Wiley and Sons, 445 pp.

Chui, C.K., 1992: *An Introduction to Wavelets*. Academic Press, 266 pp.

Cornman, L. B., C.S. Morse, G. Cuning, 1995: Real-time estimation of atmospheric turbulence severity from in-situ aircraft measurements. *J. Aircraft*, vol. 32, no. 1, 171-177

Frehlich, R. and R. Sharman, 2004: Estimates of turbulence from numerical weather prediction model output with applications to turbulence diagnosis and data assimilation. *Mon. Wea. Rev.*, in press.

Sharman, R., J. Wolff, and G. Wiener, 2004: Description and evaluation of the second generation Graphical Turbulence Guidance forecasting system. *11<sup>th</sup> Conference on Aviation, Range and Aerospace Meteorology*, Hyannis, MA.

Smalikho, I.N., 1997: Accuracy of the turbulent eddy dissipation rate from the temporal spectrum of wind velocity fluctuations. *Atmos. Oceanic Opt.*, Vol. 10, no. 8, 559-563.

Williams, J., L. Cornman, D. Gilbert, S. G. Carson, and J. Yee, 2004: Improved remote detection of turbulence using ground-based Doppler radars, *11<sup>th</sup> Conference on Aviation*,

*Range and Aerospace Meteorology*,  
Hyannis, MA.

Wingrove, R.C. and R.E. Bach, 1994:  
Severe turbulence and maneuvering from  
airline flight records. *J. Aircraft*, vol. 31, no.  
4, 753-760.